



Winter and spring variation in sources, chemical components and toxicological responses of urban air particulate matter samples in Guangzhou, China



Mo Yang^{a,b}, Pasi Jalava^a, Xin-Feng Wang^c, Michael S. Bloom^{b,d}, Ari Leskinen^{e,f}, Henri Hakkarainen^a, Marjut Roponen^a, Mika Komppula^e, Qi-Zhen Wu^b, Shu-Li Xu^b, Li-Zi Lin^b, Ru-Qing Liu^b, Li-Wen Hu^b, Bo-Yi Yang^b, Xiao-Wen Zeng^b, Yun-Jiang Yu^{g,*}, Guang-Hui Dong^{b,**}

^a Department of Environmental and Biological Science, University of Eastern Finland, Yliopistoranta 1, P.O. Box 1627, FI-70211 Kuopio, Finland

^b Guangdong Provincial Engineering Technology Research Center of Environmental Pollution and Health Risk Assessment, Department of Occupational and Environmental Health, School of Public Health, Sun Yat-sen University, Guangzhou 510080, China

^c Environment Research Institute, Shandong University, Qingdao 266237, China

^d Department of Global and Community Health, George Mason University, Fairfax, VA, USA

^e Finnish Meteorological Institute, Yliopistoranta 1, P.O. Box 1627, FI-70211 Kuopio, Finland

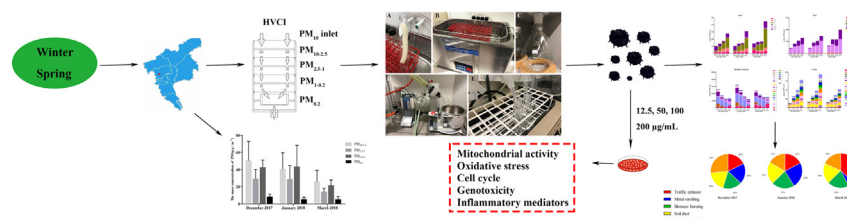
^f Department of Applied Physics, University of Eastern Finland, Yliopistoranta 1, P.O. Box 1627, FI-70211 Kuopio, Finland

^g State Environmental Protection Key Laboratory of Environmental Pollution Health Risk Assessment, South China Institute of Environmental Sciences, Ministry of Environmental Protection, Guangzhou 510655, China

HIGHLIGHTS

- Winter PM levels were high and caused severe cytotoxicity and oxidative damage.
- Spring PM had more ions, and biomass burning was the main source.
- PM components and sources led to strong variations in toxic responses.

GRAPHICAL ABSTRACT



ARTICLE INFO

Editor: Jianmin Chen

Keywords:

Urban PM
Season
Components
Sources
Toxicological responses

ABSTRACT

The sources and chemical components of urban air particles exhibit seasonal variations that may affect their hazard-ousness to human health. Our aims were to investigate winter and spring variation in particulate matter (PM) sources, components and toxicological responses of different PM size fractions from samples collected in Guangzhou, China. Four size-segregated PM samples (PM_{10-2.5}, PM_{2.5-1}, PM_{1-0.2}, and PM_{0.2}) were collected separately during winter (December 2017 and January 2018) and spring (March 2018). All PM samples were analyzed for chemical components and characterized by source. RAW 264.7 macrophages were exposed to four doses of PM samples for 24 h. Cytotoxicity, oxidation, cell cycle, genotoxicity and inflammatory parameters were tested. PM concentrations were higher in the winter samples and caused more severe cytotoxicity and oxidative damage than to PM in the spring samples. PM in winter and spring led to increases in cell cycle and genotoxicity. The trends of size-segregated PM components were consistent in winter and spring samples. Metallic elements and PAHs were found in the largest concentrations in winter PM, but ions were found in the largest concentrations in spring PM. metallic elements, PAHs and ions in size-segregated PM samples were associated with most toxicological endpoints. Soil dust and biomass burning were the main sources of PM in winter, whereas traffic exhaust and biomass burning was the main source with

* Correspondence to: Y.-J. Yu, State Environmental Protection Key Laboratory of Environmental Pollution Health Risk Assessment, South China Institute of Environmental Sciences, Ministry of Environmental Protection, 16 Ruihe Road, Huangpu District, Guangzhou 510655, China.

** Correspondence to: G.-H. Dong, Guangdong Provincial Engineering Technology Research Center of Environmental Pollution and Health Risk Assessment, Department of Occupational and Environmental Health, School of Public Health, Sun Yat-sen University, 74 Zhongshan 2nd Road, Yuexiu District, Guangzhou 510080, China.

E-mail addresses: yuyunjiang@scies.org (Y.-J. Yu), donggh5@mail.sysu.edu.cn (G.-H. Dong).

of spring PM. Our results suggest that the composition of PM samples from Guangzhou differed during winter and spring, which led to strong variations in toxicological responses. The results demonstrate the importance of examining a different particle sizes, compositions and sources across different seasons, for human risk assessment.

1. Introduction

Over the past four decades, China has experienced unprecedented urbanization and industrialization, but the concomitant increase in air pollution has become a serious public health problem (Feng et al., 2022). Particulate matter (PM) air pollution was China's fourth most important risk factor for death and disability-adjusted life years in Global Burden of Diseases, Injuries, and Risk Factors Study (GBD) 2017 (Zhou et al., 2019). The Pearl River Delta (PRD) region is one of the fastest-growing regions in south China, with some of the greatest burdens of health risks associated with energy production-related air pollution (Fang et al., 2019; Wang et al., 2019). From 2004 to 2013, 32,900–45,300 premature deaths were attributed to outdoor fine particles with aerodynamic diameter $<2.5 \mu\text{m}$ ($\text{PM}_{2.5}$) annually in the PRD region (Lu et al., 2017). Annual economic losses were estimated to be 1.55–29.2 billion Chinese Yuan (RMB) in the PRD region, due to premature mortality and chronic respiratory disease caused by P (PM with an aerodynamic diameter $<10 \mu\text{m}$ (PM_{10})) (Huang et al., 2012).

The Guangdong-Hong Kong-Macao Greater Bay Area is one of China's most dynamic economic regions.

Guangzhou is the central city of the Bay Area (Supplementary materials Fig. A.1), and had a population of approximately 18.7 million permanent residents in 2021 (approximately 20 % of the total population of the Bay Area). Therefore, it is imperative to understand the impact of Guangzhou's PM pollution to the health of the population under the influence of the Bay Area economy.

Urban atmospheric PM is a complex mixture of different chemical and biological components emitted from different sources, including pollen, bacterial, soot, heavy metals and polycyclic aromatic hydrocarbons (PAHs) (Kalisa et al., 2019; Kim et al., 2021; Rönkkö et al., 2021). These particles undergo chemical and physical transformations in the atmosphere largely dependent on season and time (Longhin et al., 2013; Manzano-León et al., 2016; Rönkkö et al., 2018). A large number of studies show that PM composition and toxicity vary with time, location, particle size and source, in addition to particle mass concentration (Jalava et al., 2015a; Jin et al., 2019; Kroll et al., 2013; Longhin et al., 2020; Park et al., 2018; Velali et al., 2018). The causal relationships between PM components and mechanisms of toxicity are still unclear. Current air quality guidelines assume that particles are uniformly toxic, ignoring the chemical components and their interactions. Yet, panel studies have reported significant correlations between different atmospheric fraction sizes and different $\text{PM}_{2.5}$ constituents with different levels of blood lipids, blood pressure and left ventricular voltage in healthy adults (Feng, 2021; Feng et al., 2021; Guo et al., 2021; He et al., 2021). However, the knowledge concerning the association between human health effects and PM components of different PM fraction sizes remains limited. To foster prevention, additional multidisciplinary efforts are still needed to identify most relevant PM components and emission sources related to the human health.

In this study, we investigated associations between of seasonal conditions, chemical composition and dominant PM emission sources on toxicological responses to size-segregated PM exposure in RAW 264.7 macrophages. Our aims were to investigate winter and spring variations in PM composition, emission sources, and toxicological responses of different PM size fractions from air samples in Guangzhou, China.

2. Materials and methods

2.1. PM sampling, collection and extraction

PM samples were collected at the North campus of Sun Yat-sen University, in Guangzhou, China, with a high-volume cascade impactor (HVC) at

a sampling rate of 850 L/min (Jalava et al., 2015a). The PM sampling was located on the roof of a ten-story building, without nearby higher structures. We collected $\text{PM}_{10-2.5}$, $\text{PM}_{2.5-1}$, $\text{PM}_{1-0.2}$, $\text{PM}_{0.2}$ samples during December 2017, January 2018 and March 2018. High performance liquid chromatography (HPLC) grade methanol was used to wash the polyurethane foam (PUF) sampling materials and fluoropore filters three times. The sampling filters were weighed before and after sampling three times with an analytical balance. Detailed sampling information is provided in Supplementary material Table A7. After sampling and weighing, filter was placed into a clean glass tube, filled with 50 mL methanol (HPLC) and subjected to ultrasound for $3 \times 30 \text{ min}$ (temperature below $35 \text{ }^\circ\text{C}$). We then combined the same size fraction samples and evaporated excess methanol at $35 \text{ }^\circ\text{C}$ and 150 mbar in the rotary evaporator. The concentrated suspension was divided into several small glass tubes by particulate mass and dried under nitrogen (99.99 %). The particulate samples were stored at $-20 \text{ }^\circ\text{C}$ until the analysis of chemical components and toxicological experiments. We followed the same procedure was for blank samples.

2.2. PM size distribution and number concentration monitoring

The PM size distribution and total number concentration of 10 nm – $10 \mu\text{m}$ particles were monitored using a Nanoscan SMPS (scanning mobility particle sizer Model 3910, TSI incorporated, USA) and an Optical Particle Sizer Spectrometer (Model 3330, TSI incorporated, USA) in the same location as the PM sampler. We combined the size distributions from the two instruments according to procedures described by Alas et al. (2019), and calculated averages over the HVC sampling times. We also used a weather transmitter to monitor wind speed and direction, precipitation, temperature and relative humidity at the PM sampling location (WXT 520, VAISALA, Finland).

2.3. PM chemical components analysis

PM samples were analyzed for the following ions by ion chromatography using a Dionex ICS-1100 (Thermo Fisher, USA): sodium (Na^+), ammonium (NH_4^+), potassium (K^+), lithium (Li^+), magnesium (Mg^{2+}), calcium (Ca^{2+}), fluoride (F^-), chloride (Cl^-), bromine (Br^-), nitrite (NO_2^-), nitrate (NO_3^-), sulfate (SO_4^{2-}) and phosphate (PO_4^{3-}). PM samples were placed in ultrapure water (10 mL), shaken horizontally at 1500 rpm for 15 min, then sonicated for 20 min at low temperature, and centrifuged at 4500 rpm for 10 min. Extract supernatant was transferred by syringe (1 mL) and filtered into a tube using a millipore 0.45 μm syringe filter. An Ionpac AS19 (4*250 mm) chromatographic column was used for separating anions, and an Ionpac CS12A (4*250 mm) chromatographic column was used for separating cations. The detection limits are shown in Supplementary materials table A1.

Trace elements were analyzed by inductively coupled plasma mass spectrometry using a Thermo Fisher-iCAP RQ ICP-MS (Thermo Fisher, USA), including: beryllium (Be), sodium (Na), magnesium (Mg), aluminum (Al), silicon (Si), potassium (K), calcium (Ca), vanadium (V), chromium (Cr), manganese (Mn), iron (Fe), Cobalt (Co), nickel (Ni), copper (Cu), zinc (Zn), arsenic (As), selenium (Se), strontium (Sr), yttrium (Y), cadmium (Cd), stannum (Sn), antimony (Sb), barium (Ba), cerium (Ce), thallium (Tl), lead (Pb), uranium (U).

PM samples were eluted with 3 mL of an acid mixture (5.55 % nitric acid HNO_3 + 16.55 % hydrochloric acid HCl + 77.9 % ultrapure water), and the mixture was transferred to digestion tube. All digestion tubes were placed into a nitrification tray and the nitrification instrument (Milestone-Ultra CLAVE, Italy) and condensate water circulation machine were activated. The nitrification tray was placed in the nitrification instrument and the nitrogen gas flow was allowed until the pressure exceeded

50 bars. PM samples were heated until the temperature reached +180 °C, which was maintained 20 min. After nitrification, the nitrification tubes were removed from the instrument, and each sample was filtered into a tube, fixed to 5 mL with ultrapure water, and analyzed using ICP-MS. The detection limits are shown in Supplementary materials table A2.

Polycyclic aromatic hydrocarbons (PAHs) were analyzed by gas chromatography with tandem mass spectrometry using an Agilent GC-MS 7890B-5977A (Agilent, USA), in the selected ion monitoring (SIM) mode. An Agilent HP-5MS (30 m*0.25 mm*0.25 μm) column was to separate the compounds. A total of 18 PAHs were analyzed, including: Naphthalene (NA), Acenaphthene (AC), Acenaphthylene (ACL), Fluorene (FL), Phenanthrene (PHE), Anthracene (AN), Fluoranthene (FA), Pyrene (PY), Benzo(a)anthracene [B(a)A], Chrysene (CHR), Benzo(b)fluoranthene [B(b)FA], Benzo(k)fluoranthene [B(k)FA], Benzo(j)fluoranthene [B(j)FA], Benzo(e)pyrene [B(e)P], Benzo(a)pyrene [B(a)P], Indeno(1,2,3-cd)pyrene (IP), Dibenzo(a,h)anthracene [DB(a,h)A] and Benzo(g,h,i)perylene [B(g,h,i)P]. The PM sample was mixed into 10 mL of "mixture A" (dichloromethane: methanol 97:3), an internal standard was added, and the mixture was sonicated for 20 min. The samples were transferred to a sample bottle, and evaporated by nitrogen to 1 mL. 10 mL of mixture A was added to 1 mL of nitrogen blown concentrate, and repeated the steps of above sonication and nitrogen blowing. The addition of 10 mL of mixture A, sonication and nitrogen evaporation were repeated three times, and the PM samples were evaporated by nitrogen to 0.5 mL. The 0.5 mL concentrate was added to the activated anhydrous sodium sulfate chromatography column, washed five times with eluent (dichloromethane: n-hexane = 1:1), and 15 mL of sample solution was obtained. Sample solution was evaporated by nitrogen to 1–2 mL, then added to the activated silica gel purification chromatography column, and the elution and nitrogen evaporation steps were repeated. Finally, the PM sample was dried with nitrogen, dissolved into 300 μL n-hexane and analyzed on the GC-MS. The detection limits are shown in Supplementary materials table A3.

2.4. Source appointment by positive matrix factorization (PMF) model

A positive matrix factorization receptor model (USEPA, PMF v5.0) was used to identify the major sources of PM in different size ranges and to quantify the contributions from each source. Two files are required as the PMF model inputs - the concentration data and the corresponding uncertainty data. These values were determined as follows (Arruti et al., 2011; Polissar et al., 1998):

For concentration values below the detection limits:

$$x_{ij} = \frac{DL_i}{2}, \sigma_{ij} = \frac{5DL_i}{6} \quad (1)$$

For concentration values beyond the detection limits:

$$x_{ij} = c_{ij} \quad (2)$$

$$\text{If } x_{ij} \leq 3DL_i, \sigma_{ij} = \frac{DL_i}{3} + 0.2 \times c_{ij}; \quad (3)$$

$$\text{If } x_{ij} > 3DL_i, \sigma_{ij} = \frac{DL_i}{3} + 0.1 \times c_{ij}; \quad (4)$$

where x_{ij} is the concentration value of the species i for the sample j , DL_i is the detection limit of the species i , σ_{ij} is the uncertainty value corresponding to the concentration x_{ij} , and c_{ij} is the measured concentration. Note that the sample data with missing values were not included in the input data file. The predicted concentration and the observed concentration of all PM samples were relatively matched (Fig. A.2). The PMF model was run 40 times and the optimal result was chosen as outputs based on the minimum bootstrap error. The bootstrap error estimation was determined by minimum Q/Qexp value (Li et al., 2020; Zhang et al., 2018).

In this study, a total of 41 variables covering the mass concentration of PM (i.e. PM_{10-2.5}, PM_{2.5-1}, PM_{1-0.2}, or PM_{0.2}), seven ions including sulfate,

nitrate, chloride, ammonium, sodium, potassium, and calcium, fifteen elements including Si, Al, Fe, Ba, Sr, Mn, Cr, Ni, Cu, Zn, As, Cd, Ph, Sn, and Sb, and seventeen PAHs including NA, ACL, AC, FL, AN, PHE, FA, FY, BaA, CHR, BbFA, BkFA, BjFA, BeP, IO, DBaA, and BghiP were selected as the input of the PMF model. There were 128 samples (i.e., 128 data sets) available to run the PMF model. Factors were identified and interpreted according to *a priori* criteria, including investigation of the retrieved factor profiles for distinct chemical signatures and comparison of the time series of the factors with tracers. To obtain optimal source apportionment results, three to eight factors were tested and evaluated. The selection for the proper number of factors was based on an integrated analysis of the Q/Qexp, scaled residuals, the residual time series as a function of the number of factors, the variability of each variable attributed to the source from the bootstrap approach, and the reasonableness of the resolved factors as individual sources. Finally, a five-factor solution was chosen. Note that solutions with less than five factors showed obvious increase in scaled residuals and the combined metal smelting, biomass burning, and coal combustion related factors, while solutions with greater than five factors revealed a split of the biomass burning related factor and the traffic factor.

2.5. Cell culture and PM exposure

Mouse macrophage from the RAW 264.7 cell line were obtained from American Type Culture Collection (ATCC). RAW 264.7 macrophages were cultured in RPMI 1640 cell culture medium (Life Technologies) supplemented with 10 % heat-inactivated fetal bovine serum (FBS)(Sigma, USA), 1 % L-Glutamine and 1 % Penicillin-streptomycin (Life Technologies, USA) in a 5 % CO₂ atmosphere at 37 °C. During the experiments, the cell suspension was diluted to 3 × 10⁵ cells/mL and cultured on 12-well plates (Costar, Corning, NY, USA) for 24 h to allow the cells to adhere and divide. One hour before the PM exposure experiment, fresh medium was exchanged and cells were allowed to stabilize.

PM sample tubes were treated in ultrasonic bath for 30 min to suspend the particulate samples into pyrogen free water (Sigma W1503, USA) and dimethyl sulfoxide (DMSO) (final concentration 0.3 % v/v at dose 150 mg/mL in cell culture medium) at a concentration of 5 mg/mL before exposure. The DMSO concentration was tested as non-toxic during the analyses. The cells were treated with a control and four doses (12.5, 50, 100 and 200 μg/mL) of each PM sample for 24 h. All experiments were carried out in triplicate with at least three replicates. After the PM exposure, we collected and stored the cell culture medium at -80 °C, and recovered cells adhering to the bottom of each well using a cell scratcher with 600 μL cold phosphate buffered saline (PBS). We then centrifuged the tubes (8000 rpm, 5 min, 4 °C), removed the supernatant and resuspended the cells with a proper volume of cold PBS. Several toxicological analyses were conducted to investigate pathologic responses, including inflammation, cytotoxicity and genotoxicity.

2.6. MTT test

Cellular mitochondrial activity was detected with the MTT-test using 96-well plates. After the PM exposure, we added 25 μL of MTT-solution to each well, incubated for 2 h at 37 °C, and added 100 μL of sodium dodecyl sulfate (SDS) buffer to each well and incubated overnight at 37 °C. The absorbance was detected with a spectrophotometric plate reader and recorded at 540 nm. Cell viability was calculated as a percentage response relative to the control group. Potential interference of the PM samples themselves with the method was tested and ruled out.

2.7. Cell membrane integrity and DCF

Cell membrane integrity was tested by the propidium iodide (PI) exclusion assay and intracellular oxidative stress by the 2',7'- dichlorofluorescein (DCF) assay. After the PM exposure and cell collection procedure, we resuspended cells with 400 μL cold PBS. We took 100 μL of cells to 96-well plate, and added 8 μL of DCF solution to each well. We immediately detected and

recorded the absorbance with the spectrophotometric plate reader at 485 nm. We detected the absorbance twice more, at 30 min intervals, after incubation at 37 °C. We then added 7.2 μL PI solution to each well, stirred briefly with a plate shaker and incubated for 20 min at 37 °C. The absorbance was detected using a spectrophotometric plate reader and recorded at 540 nm. After the fluorescence measurement, we added 20 μL of 10 % Triton X-100 to each well and incubated 20 min at room temperature covered with foil on a plate shaker. We then repeated the measurement once.

2.8. Cell cycle

After the PM exposure, we fixed collected cells in 4 mL cold 70 % ethanol. After fixation, we centrifuged the cells (480 g, 5 min, 4 °C) and removed the ethanol. We then washed (1 mL cold PBS) and resuspended the cells in 250 μL cold PBS, added 7.5 μL RNase A (10 mg/mL) to each tube, vortexed the cells and incubated at 50 °C for one hour. Then, we added 4 μL PI solution, vortexed the cells and incubated at 37 °C for 30 min. The cell cycle phases were analyzed by flowcytometric analysis with a BD FACSCanto™ II (BD Biosciences, San Jose, CA USA).

2.9. Comet assay

After PM exposure and cell collection, we resuspended cells with 400 μL cold PBS. We mixed 60 μL of cells into 540 μL of freeze medium (40 % of filtrated FBS, 50 % RPMI, 10 % DMSO) and froze the cells at -80 °C. Samples were thawed and centrifuged (8000 rpm, 5 min, 4 °C). We retained 50 μL medium in the tube, mixed 20 μL of cell suspension into 80 μL of 0.5 % low melting point agarose (LMPA) and spread 80 μL of this cell LMPA mixture onto microscope slides with 1 % normal melting point agarose (NMPA). We added a glass cover plate onto the microscope slide, and set the microscope slides on an ice block for 5 min before removing the glass cover plate. We added lysis buffer on the microscope slides for 1 h at 4 °C, and then placed the microscope slides into an electrophoresis chamber, added electrophoresis buffer and incubated the slides in complete darkness for 40 min. After that, we set the electrophoresis for 20 min at 24 V/300 mA, removed the microscope slides and rinsed 3 times with neutralization buffer. We fixed the DNA on the microscope slides using 99 % ethanol for 10 min and then removed the ethanol. We dried the microscope slides overnight at the room temperature and stored in dry and dark conditions. At last, we pipetted 75 μL of diluted ethidium bromide dye onto the microscope slides, covered with a glass cover plate, waited 30 min for dye to allow for DNA binding and imaged the slides. We analyzed the nuclei in ethidium bromide (100 cells per dose) using a special image analysis system (Comet assay IV, Perceptive Instruments Ltd., Suffolk, UK). Tail intensity was used as the parameter in the statistical analysis.

2.10. Measurement of inflammatory mediators

Tumor necrosis factor alpha (TNF- α) and macrophage inflammatory protein 2 (MIP-2) in cell culture medium were immunochemically analyzed according to manufacturers' recommendations using commercial enzyme linked immunosorbent assay (ELISA) kits (R&D Systems, Minneapolis, MN, USA). Absorbance was detected with the spectrophotometric plate reader (BioTek, SYNERGY H1, USA) and recorded at 450 nm. ELISA kits of mouse TNF- α and MIP-2 were DuoSet ELISA. Assay range of mouse TNF- α and MIP-2 were 31.2–2000 pg/mL and 15.6–1000 pg/mL, respectively.

2.11. Statistical analysis

All the cell experiment results of different groups were compared using one-way analysis of variance (ANOVA), followed by the least squared difference (LSD) method to compare paired differences between the groups. Non-parametric Spearman correlation was used to examine the association

between toxicological endpoints. A p -value <0.05 was considered to be statistically significant.

3. Results

3.1. PM concentration and wind distribution

Fig. 1 shows the calculated average concentrations of size-segregated particulate samples and wind distributions in December 2017, January 2018 and March 2018. Among all the particles, the concentration of $\text{PM}_{10-2.5}$ was the highest (50.49 $\mu\text{g}/\text{m}^3$), and $\text{PM}_{0.2}$ was the lowest (5.33 $\mu\text{g}/\text{m}^3$) (Fig. 1D). $\text{PM}_{10-2.5}$ and $\text{PM}_{2.5-1}$ concentrations decreased gradually from December 2017 to March 2018. A similar decrease was found in the monthly averages of particle size distributions as their geometric mean diameters (GMD) in the fitted unimodal lognormal distributions were 0.077, 0.068, and 0.059 μm , respectively (Fig. 2). The concentration trends of different particle sizes were similar in the winter and spring. A summary of continuous air quality measurements, temperature and relative humidity during sample collections from December 2017 to March 2018 are shown in Table 1. PM concentration was significantly higher in winter than in spring. Although the temperature in winter was lower than in spring, the relative humidity was also higher. The prevailing wind directions were north during December 2017 and January 2018, and north and south during March 2018 (Fig. 1A-C). The wind speeds were similar in winter and higher than in spring.

3.2. PM chemical composition and source

Fig. 3 shows the mass concentrations of ions, metallic elements and PAHs in size-segregated particulate samples collected in December 2017, January 2018 and March 2018. The ions and PAHs content of $\text{PM}_{0.2}$ were the greatest in winter and spring, of which K^+ was the highest cation and NO_3^- was the highest anion (Fig. 3A, B). Metallic element contents were the highest in $\text{PM}_{10-2.5}$, of which Si was the greatest (Fig. 3C). The high K^+ and NO_3^- concentrations in PM indicated the large influence of biomass burning activities during the sampling periods. Five major sources of PM were identified, including coal combustion, metal smelting, traffic exhaust, biomass burning, soil dust based on the PMF results. Specifically, as shown in Fig. A.3, the traffic exhaust related source was associated with elevated

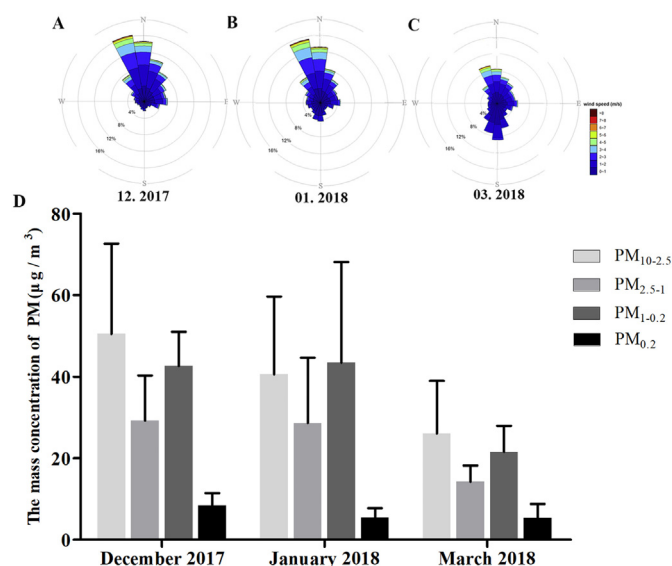


Fig. 1. Calculated average concentrations of size-segregated particulate samples and wind distributions in December 2017, January 2018 and March 2018, Guangzhou. A-C: wind distribution; D: Average size-segregated particle concentrations.

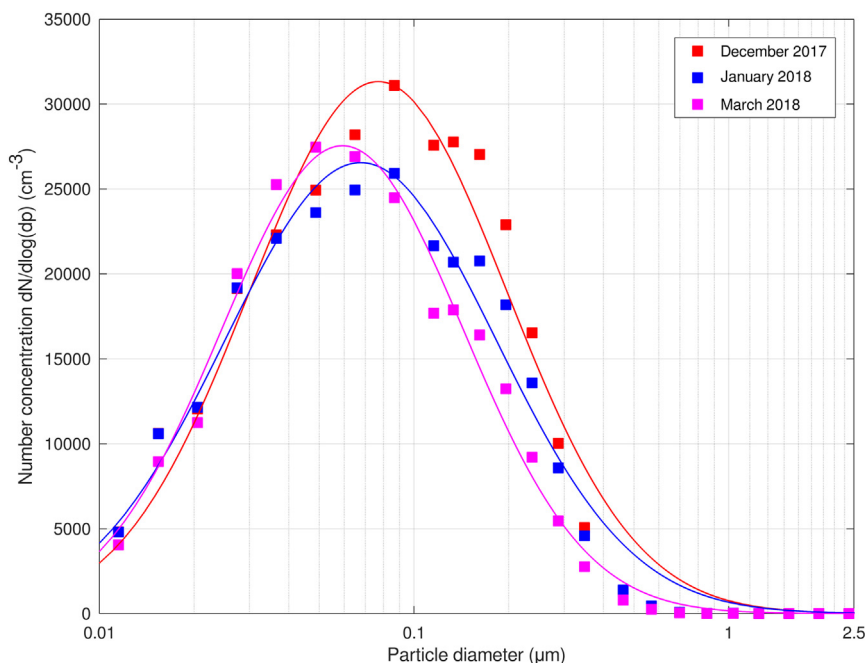


Fig. 2. Monthly averages of the ambient particle size distributions during the HVCI samplings. The solid lines represent unimodal lognormal fittings to the measured data.

concentrations and contributions of NO_3^- , Na^+ , Ca^{2+} , AC, FL, and AN. The metal smelting related source was indicated by high concentrations and contributions of Mn, Cr, Ni, Cu, Zn, and Cd. The biomass burning related source was characterized by high concentrations and contributions of K^+ , Cl^- , and NO_3^- . The soil dust source featured very high concentrations and contributions of crustal elements such as Ca^{2+} , Si, Al, and Fe. The coal combustion source was characterized by a relatively high contribution of SO_4^{2-} and elevated concentrations and contributions of B(a)A, CHR, B(b)FA, B(k)FA, B(a)P, IP, B(g,h,i)P. The variability of each factor's contribution to the individual sources generally fell in the acceptable range (Fig. A.4).

Fig. 4 shows the contributions of coal combustion, metal smelting, traffic exhaust, biomass burning and soil dust to the sources of size-segregated PM emissions. Biomass burning and soil dust were the main PM sources in winter, traffic exhaust and biomass burning were the most important contributor in PM spring (Fig. 4A-C). Soil dust was the major source of coarse particle emissions ($\text{PM}_{10-2.5}$); biomass burning was the main source of fine particles ($\text{PM}_{2.5-1}$ and $\text{PM}_{1-0.2}$); traffic exhaust was the main source of $\text{PM}_{0.2}$ (Fig. 4D). More detailed results are provided in the supplementary material Table A8.

3.3. MTT

Fig. 5 shows the mitochondrial metabolic activity of RAW 264.7 macrophages after exposure to size-segregated PM samples as assessed with the MTT test. All PM samples induced dose-dependent decreases of mitochondrial viability at three time points. The greatest cytotoxic effects were observed in December 2017 for all the PM samples, especially $\text{PM}_{10-2.5}$

Table 1

Mean of continuous air quality measurements, temperature and relative humidity during sample collection from December 2017 to March 2018, in Guangzhou.

Items	December 2017	January 2018	March 2018
$\text{PM}_{2.5}$ ($\mu\text{g}/\text{m}^3$)	75.04	83.58	55.52
PM_1 ($\mu\text{g}/\text{m}^3$)	71.03	79.43	52.44
$\text{PM}_{0.2}$ ($\mu\text{g}/\text{m}^3$)	10.30	9.25	8.04
Temperature ($^\circ\text{C}$)	16.92	15.79	20.50
Relative Humidity (%)	42.76	63.84	54.83

(Fig. 5A); the cytotoxic effects of $\text{PM}_{2.5-1}$, $\text{PM}_{1-0.2}$ and $\text{PM}_{0.2}$ in January 2018 and March 2018 were similar (Fig. 5B-D).

3.4. Intracellular oxidative potential and membrane integrity

Fig. 6 shows the intracellular oxidative responses of RAW 264.7 macrophages after exposure to size-segregated PM samples. $\text{PM}_{10-2.5}$ in December 2017 induced the strongest increase of the oxidative stress response in a dose-dependent fashion (Fig. 6A), the responses were three-fold greater compared to the control group with exposure to 100 $\mu\text{g}/\text{mL}$ and 200 $\mu\text{g}/\text{mL}$. Responses to $\text{PM}_{10-2.5}$ and $\text{PM}_{1-0.2}$ in January 2018 and March 2018 were similar (Fig. 6A, B). Exposures to $\text{PM}_{2.5-1}$ and $\text{PM}_{0.2}$ in March 2018 resulted in significantly higher responses than in December 2017 and January 2018, especially for $\text{PM}_{0.2}$ (Fig. 6B, D). Fig. A.5 shows the cell membrane integrity of RAW 264.7 macrophages after size-segregated PM samples exposure. There were no obviously changes in cell membrane integrity among compared to the control samples.

3.5. Cell cycle

Fig. 7 describes the percentages of RAW 264.7 macrophages arrested in cell cycle states after exposure to size-segregated PM samples in Sub-G1/G0 phase, G1 phase, Sub G2-M phase and G2-M phase. Among the four cell cycle phases, only the Sub G1/G0 phase was dose-dependently increased with exposure to the four size-segregated particles. Exposure to March 2018 $\text{PM}_{10-2.5}$ and $\text{PM}_{1-0.2}$ induced a significantly higher Sub-G1/G0 population than samples collected in December 2017 and January 2018 (Fig. 7A, C). Exposure to $\text{PM}_{2.5-1}$ and $\text{PM}_{0.2}$ in collected January 2018 induced a significantly higher responses than samples collected in December 2017 and March 2018 (Fig. 7B, D). Among all the PM samples, the greatest increase of Sub-G1/G0 population was observed with exposure to $\text{PM}_{1-0.2}$ collected in March 2018, and the response to the 200 $\mu\text{g}/\text{mL}$ $\text{PM}_{1-0.2}$ dose was 12.23 times greater than that of the control group (Fig. 7C).

3.6. Genotoxicity

Fig. 8 shows the genotoxicity of RAW 264.7 macrophages after exposure to size-segregated PM samples. There were monthly time-dependent

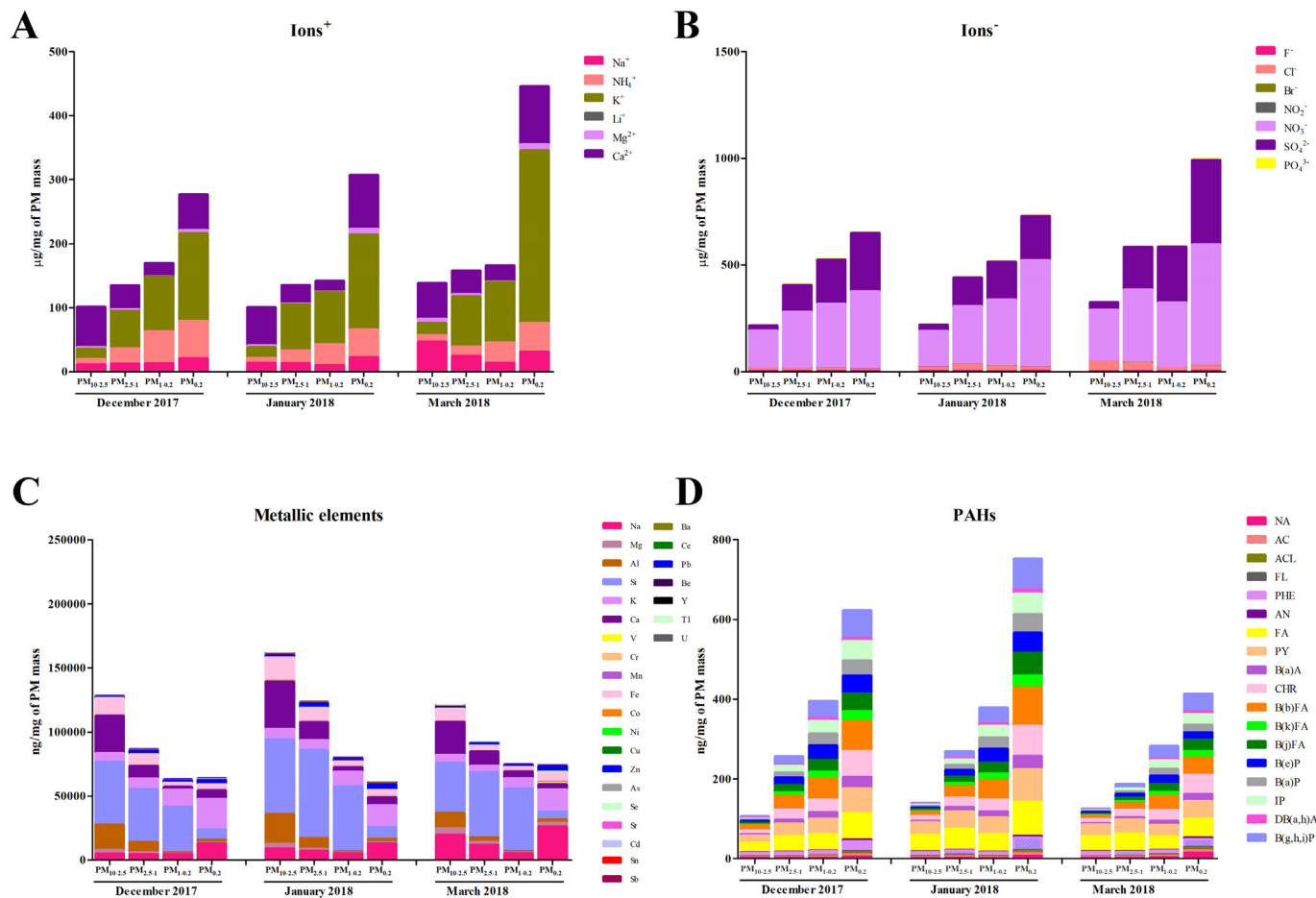


Fig. 3. Mass concentration of ions, metallic elements and PAHs in particulate samples in Guangzhou.

increases in the 200 µg/mL PM_{10-2.5} dose group in December 2017, January 2018 and March 2018 (Fig. 8A). Exposure to December 2017 PM_{2.5-1} resulted in a significantly higher response than exposure to January 2018 and March 2018 samples (Fig. 8B). The January 2018 50 µg/mL, 100 µg/mL and 200 µg/mL PM_{1-0.2} groups caused significantly higher genotoxicity than those of December 2017 and March 2018 (Fig. 8C). Exposure to December 2017 50 µg/mL, 100 µg/mL and 200 µg/mL PM_{0.2} groups resulted in significantly lower genotoxicity than those from January 2018 and March 2018 (Fig. 8D). Among all the PM samples, the most genotoxic effect was observed for the in March 2018 PM_{10-2.5} sample, for which the tail intensity in the highest dose (200 µg/mL) group was 8.81 times that of the control group (Fig. 8A).

3.7. Inflammatory mediators

Fig. 9 shows the levels of TNF-α and MIP-2 in RAW 264.7 macrophages after exposure to size-segregated PM samples. Most PM samples induced dose-dependent increases in TNF-α and MIP-2. PM_{10-2.5} (200 µg/mL), PM_{2.5-1} (100 and 200 µg/mL) and PM_{0.2} (100 µg/mL) groups in January 2018 caused significantly greater TNF-α level than their same December 2017 and March 2018 counterparts (Fig. 9A). The MIP-2 levels from exposure to December 2017 200 µg/mL PM_{10-2.5} dose group was significantly higher than from exposure to the January 2018 and March 2018 PM_{10-2.5} dose groups. Exposure to PM_{2.5-1} and PM_{1-0.2} showed time-dependent MIP-2 increases in December 2017, January 2018 and March 2018; the response to the January 2018 PM_{0.2} was significantly higher than that of December 2017 and March 2018 (Fig. 9B). Among all PM samples, PM₁₀₋

2.5 induced the greatest productions of TNF-α and MIP-2, whereas, the PM_{1-0.2} induced the least.

3.8. Associations of PM components and sources with toxicological endpoints

Table 2 shows the associations of PM components with toxicological endpoints in RAW 264.7 macrophages. For PM_{10-2.5}, ions were significantly associated with all toxicological endpoints, especially in the 50 µg/mL group; total elements were significantly associated with DNA Tail-intensity; and PAHs were significantly associated with MTT, cell cycle Sub-G1/G0 phase, DCF, TNF-α and MIP-2, especially in the 200 µg/mL group. For PM_{2.5-1}, there were significant associations between ions and total elements with nearly all the toxicological endpoints; PAHs were significantly associated with DNA Tail-intensity, DCF, TNF-α and MIP-2. For PM_{1-0.2}, ions were significantly associated with DNA Tail-intensity and MIP-2; total elements were significantly associated with MTT, Sub-G1/G0 phase, DNA Tail-intensity and DCF in the 100 µg/mL group; PAHs were significantly associated with almost all the toxicological endpoints, especially in the high dose groups. For PM_{0.2}, ions, total elements and PAHs were significantly associated with DCF in all dose groups; ions, total elements and PAHs were significantly associated with Sub-G1/G0 phase in 12.5 and 50 µg/mL groups; ions, total elements and PAHs were significantly associated with DNA Tail-intensity in 50 and 200 µg/mL groups; and ions, total elements and PAHs were significantly associated with TNF-α and MIP-2 in 100 µg/mL group and 12.5 µg/mL group, respectively. The associations between the mass fraction of PM chemicals (total, winter, spring) and toxicological endpoints were showed in the Table A4.

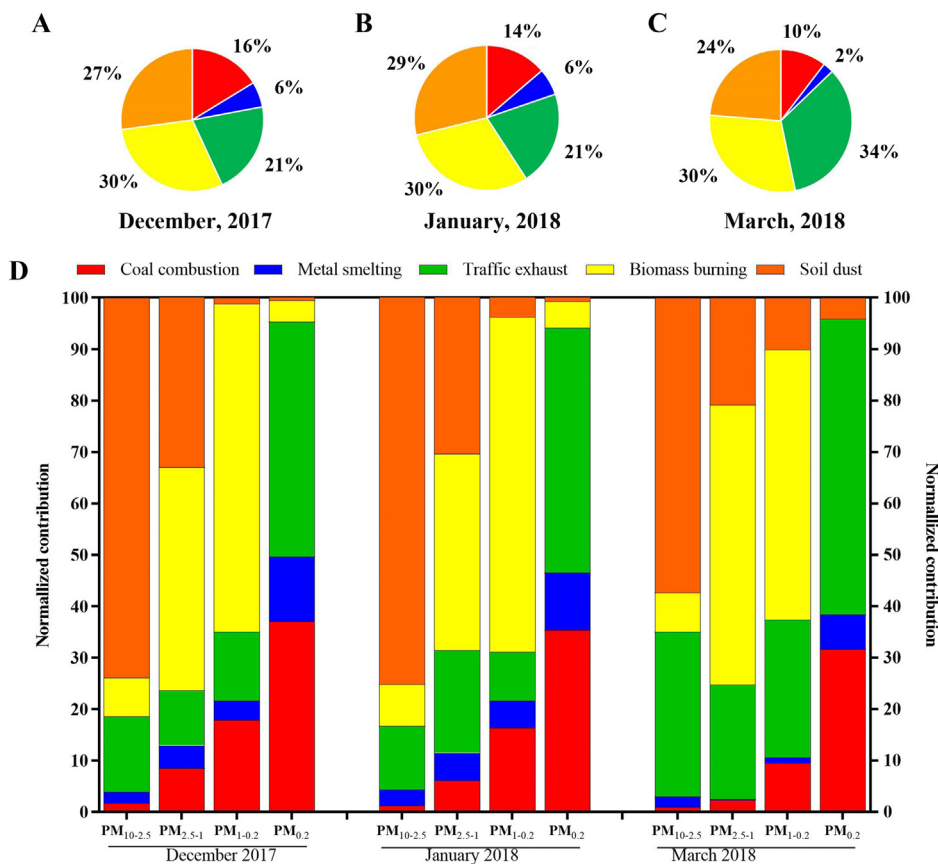


Fig. 4. Contributions of coal combustion, metal smelting, traffic exhaust, biomass burning and soil dust to the sources of size-segregated particulate samples in Guangzhou. A–C: Contributions of coal combustion, metal smelting, traffic exhaust, biomass burning and soil dust to the sources of particulate samples in December 2017, January 2018 and March 2018; D: Size-segregated particulate samples contributions in December 2017, January 2018 and March 2018.

Ions and PAHs always have similar associations with toxicological endpoints, whereas the associations of metals with toxicological endpoints were opposite to the correlation of ions or PAHs and toxicological endpoints.

The associations between the PM emission sources and toxicological endpoints are shown in supplementary material Table A5. Traffic exhaust, soil dust and coal combustion were associated with virtually all toxicology endpoints. An increase of traffic exhaust caused a decrease in cell mitochondrial activity and an increase in intracellular oxidative potential. In addition to coal burning, increases in four other PM exposure sources caused inflammatory response. Biomass burning has the smallest correlation with toxicology endpoints.

4. Discussion

In this study, we found that the PM_{10-2.5}–PM_{0.2} concentrations in Guangzhou were higher in winter than in spring. Similarly, cytotoxicity and oxidative damage from exposure to winter PM samples were higher than for spring PM samples. Exposure to spring PM samples caused an increase in Sub-G1/G0 phase changes. All PM were genotoxic, with the largest responses observed in the high-dose groups. The trends of the component mass concentrations were consistent in winter and spring PM. The concentrations were highest for metallic elements and PAHs in winter PM; whereas for ion concentrations made the largest contributions to spring-PM. PM ions, metallic elements and PAHs were associated with almost all the toxicological endpoints. Soil dust and coal combustion were important sources of the winter PM and biomass burning was the primary source of spring PM.

The total calculated concentration of Guangzhou PM_{10-2.5} to PM_{0.2} was 122.03 $\mu\text{g}/\text{m}^3$ in winter and 66.61 $\mu\text{g}/\text{m}^3$ in spring, from which the

majority were PM_{10-2.5} (winter: 44.14 $\mu\text{g}/\text{m}^3$; spring: 26.08 $\mu\text{g}/\text{m}^3$) and PM_{1-0.2} (winter: 43.13 $\mu\text{g}/\text{m}^3$; spring: 21.55 $\mu\text{g}/\text{m}^3$). The seasonal average PM_{2.5} concentration was the highest in winter and the lowest in summer. Compared with the rainy seasons (spring and summer), PM_{2.5} levels in PRD rural areas typically doubled during the dry seasons (autumn and winter) due to frequent precipitation scavenges aerosols (Griffith et al., 2015; Lai et al., 2016). This is consistent with the higher PM concentrations in winter than in spring in this study. At present, the concentrations of PM detected by atmospheric monitoring stations in China and most studies are mainly PM₁₀ and PM_{2.5}. Although the concentration trends for particles with different sizes were similar during the same day in this study, more monitoring data are needed for concentrations of small particle sizes.

Oxidative stress plays a vital role in driving the health effects induced by air pollution (Jalava et al., 2006; Kelly, 2003). Oxidative damage from PM_{10-2.5} were greatest in December 2017 in this study. Interestingly, exposure to PM_{10-2.5} collected in January 2018, during the Guangzhou winter, did not show strong oxidative damage, even with other particle sizes. Moreover, exposure to PM_{0.2} collected in March 2018, during the Guangzhou spring, caused strong oxidative damage. The exact components and mechanisms leading to oxidative stress following PM exposure have not been determined. The chemical composition of particles is one of the key factors affecting their toxicity (Jalava et al., 2006). Production of oxidants (directly induced by air pollution particles or by host responses to particles) appears to underlie the biological effects of exposure (Ghio et al., 2012). Direct oxidation from air pollution particles is attributed to the organic and metallic components (Ghio et al., 2012; Hu et al., 2021; Samet et al., 2020). Both organic compounds and metals generate oxidative stress by depleting antioxidants through a series of reactions (Ghio et al., 2012). In this study, metallic elements and PAHs occurred at modestly higher concentrations in January 2018 PM_{10-2.5}

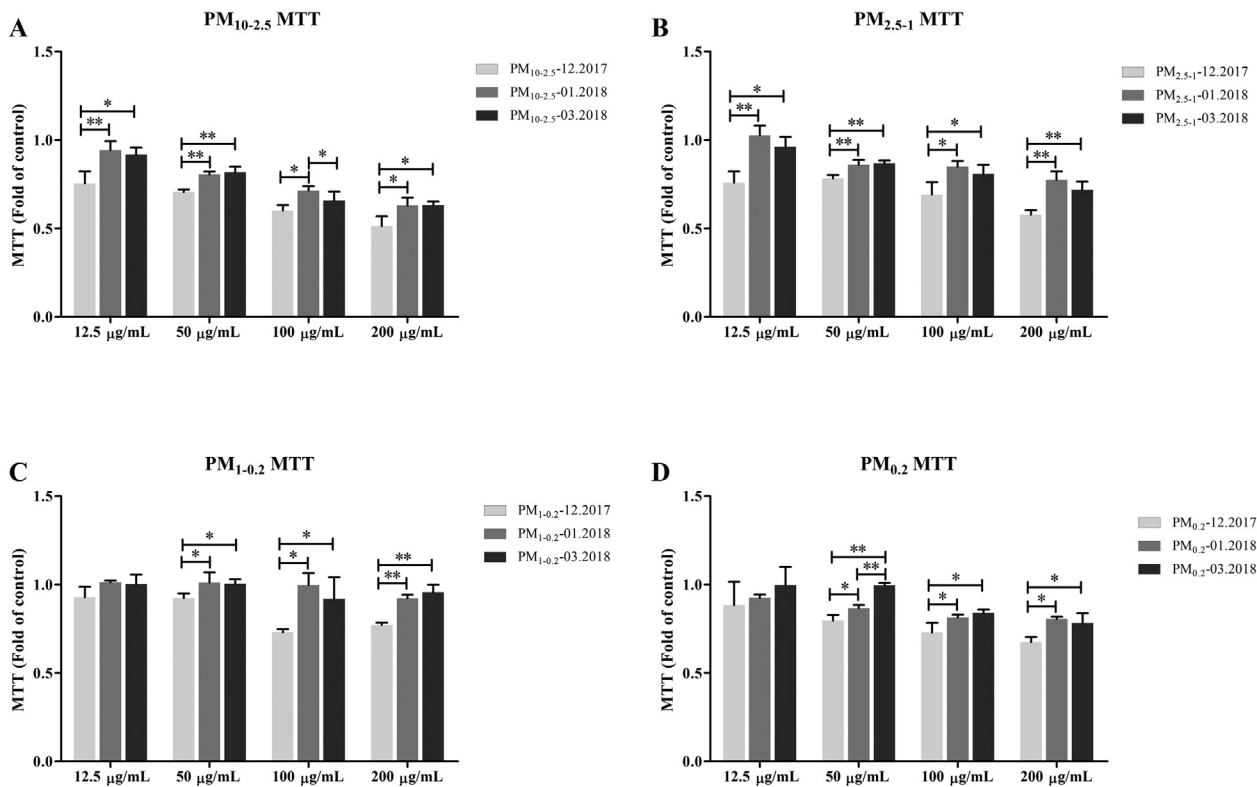


Fig. 5. Mitochondrial activity of RAW 264.7 macrophages after exposure to four doses of size-segregated particulate samples in December 2017, January 2018 and March 2018 as assessed with the MTT test. * $P < 0.05$. ** $P < 0.001$.

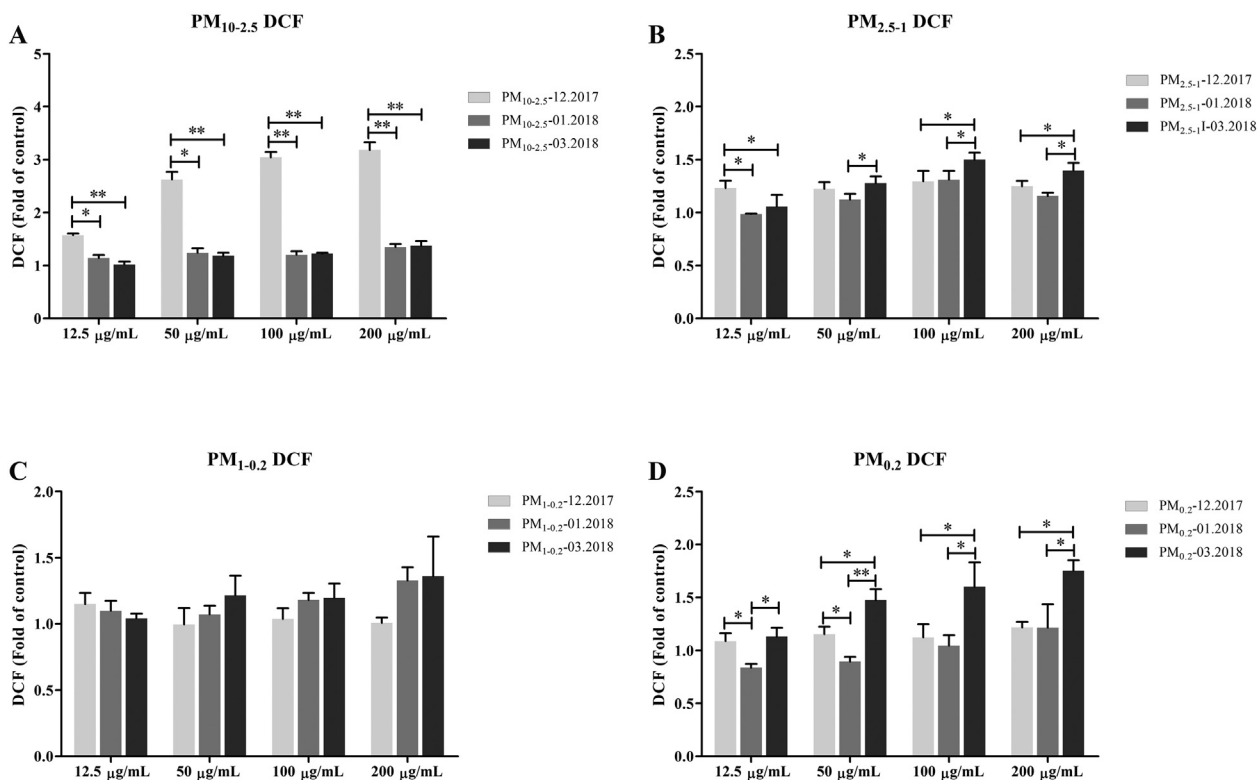


Fig. 6. Intracellular oxidative potential of RAW 264.7 macrophages after exposure to four doses of size-segregated particulate samples in December 2017, January 2018 and March 2018 as measured by DCF assay. * $P < 0.05$. ** $P < 0.001$.

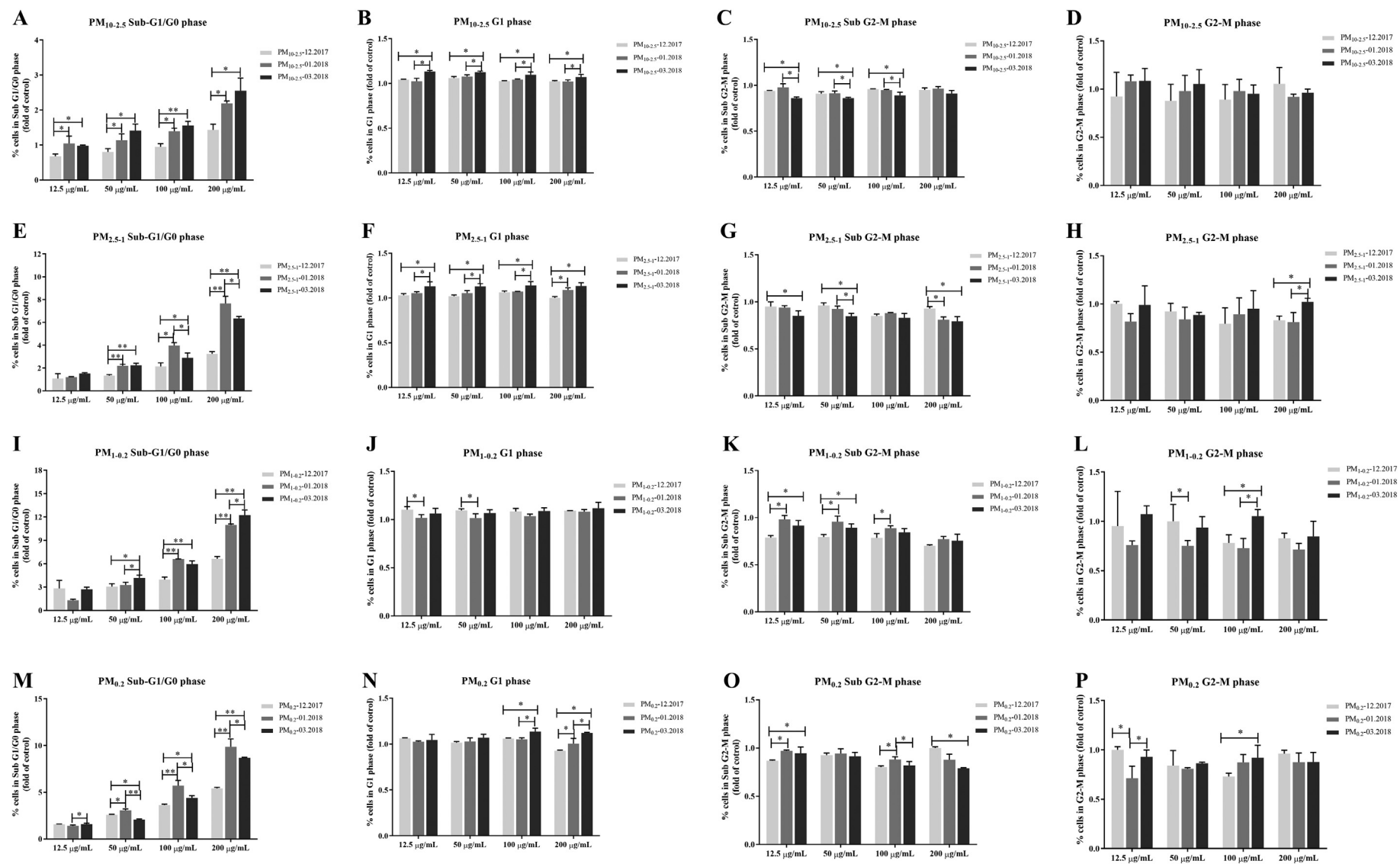


Fig. 7. Cells with severe DNA damage as measured by flowcytometric cell cycle phase analysis on ethanol-fixed and permeabilized PI-stained RAW 264.7 macrophages after exposure to four doses of size-segregated particulate samples in December 2017, January 2018 and March 2018. * $P < 0.05$. ** $P < 0.001$.

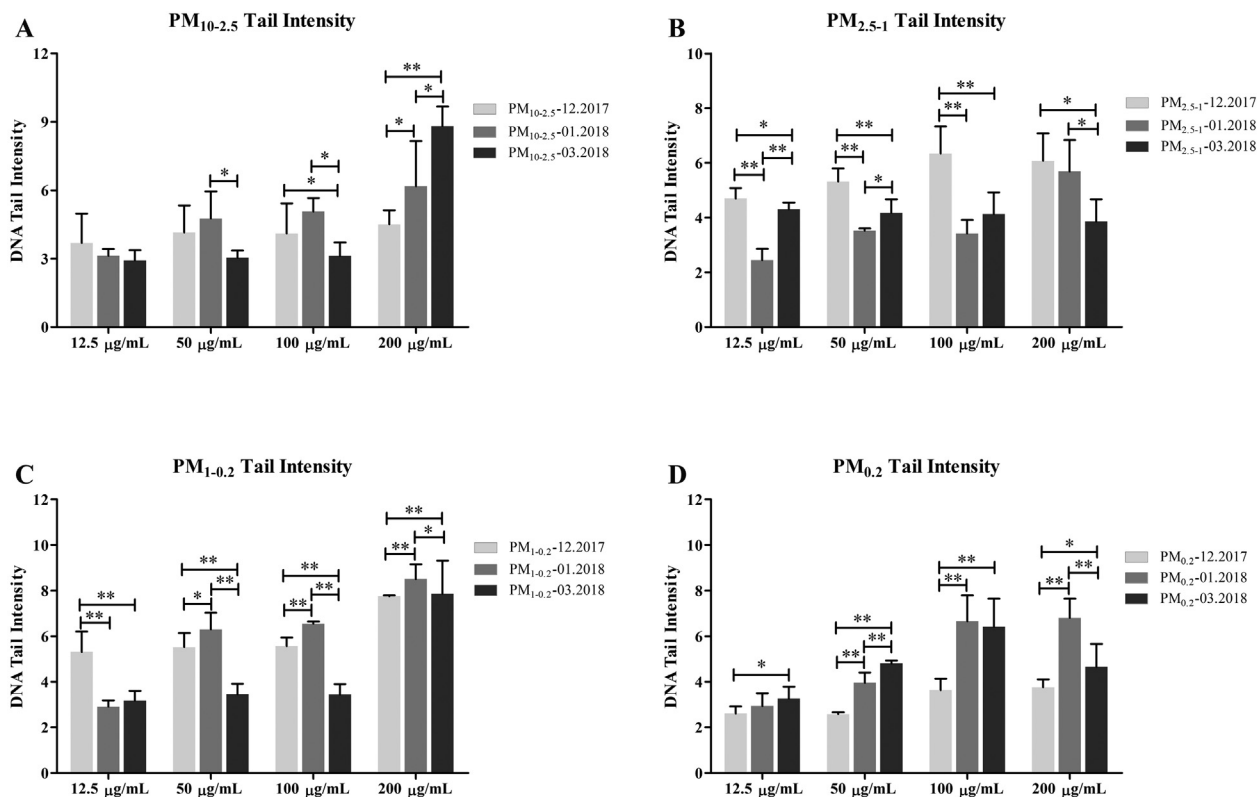


Fig. 8. Genotoxicity of RAW 264.7 macrophages after exposure to four doses of size-segregated particulate samples in December 2017, January 2018 and March 2018, reported as averaged median percentage of DNA in tail. * $P < 0.05$. ** $P < 0.001$.

than in December 2017 particles, and there were fewer metallic elements and PAHs in March 2018 PM_{0.2} than in January 2018. A study in Nanjing found that PM_{10-2.5} exposure elicited the strongest oxidative damage, but there was no significant difference in oxidative damage caused by PM_{10-2.5} in August and October 2013, even though the particles in October had more metals and PAHs (Rönkkö et al., 2018). Song et al. found that winter PM_{2.5} with a higher concentration of PAHs did not cause more severe cellular oxidative damage than summer PM_{2.5} in Guangzhou (Song et al., 2020). This suggests that although metal elements and PAHs are important contributors in PM exposure-induced oxidative stress, other factors also play a role. Previous studies have also found that metals and organic compounds are important components of PM-induced oxidative damage (Ghio et al., 2012; Hu et al., 2021; Yang et al., 2016), however, different metals and organic compounds are likely to play different roles in causing oxidative damage. Therefore, the different distributions of PM components may in part explain differences in the oxidative damage from PM exposure of with different sizes, in different cities, and during different seasons.

In addition to the direct production of oxidants from organic and metallic components, cellular responses also contribute to oxidative stress following PM exposure (Ghio et al., 2012). The production of reactive oxygen species occurs in mitochondria, cell membranes, phagosomes, and endoplasmic reticulum (Ghio et al., 2012). We found that significant negative correlations for intracellular oxidative potential (DCF) and mitochondrial activity (MTT) with most PM; DCF and cell membrane integrity was significantly negatively correlated only in PM_{0.2} (supplementary material, Table A6). This result indicates that PM exposure caused a decrease in mitochondrial activity and an increase in intracellular oxidative potential, but did not destroy the integrity of the cell membrane. There are few studies on the role of ions in PM-induced oxidative damage, but results have shown water-soluble ions as a potential source of PM-mediated toxicity (Park et al., 2022). Although we found no further evidence that ions in PM influence intracellular oxidative potential, the effect of ions on other

toxicological endpoints (Jalava et al., 2015b) may indirectly contribute to oxidative damage.

Large numbers of RAW 264.7 macrophages in the Sub-G1/G0 population indicates excess DNA repair capacity and disrupted replication. In this study, all PM exposure caused dose-dependent increase in RAW 264.7 Sub-G1/G0 population. Interestingly, the January 2018 PM produced a larger Sub-G1/G0 population than the December 2017 PM, during the same winter. This may be due to higher PAH concentrations in the January 2018 PM. Similar results were found in a study from Nanjing (Rönkkö et al., 2018). PAHs in the environment can cause DNA damage and affect the cell cycle (Bai et al., 2017). The Sub-G1/G0 population caused by all PM was greater than in winter in spring. Although PAHs in spring PM was not as high as that in winter, there was a significant positive correlation between PAHs and the Sub-G1/G0 population in this study. There is also evidence that complex PAH mixtures have non-additive and inhibitory effects on genotoxicity and DNA damage (Genies et al., 2016). The structural features of PAHs and their derivatives lead to dramatic differences in cellular responses (Motoyama et al., 2009). Therefore, extensive experiments are still needed to investigate the mechanisms by which PM induces genotoxicity and cell cycle.

Although the four particle sizes in winter and spring were genotoxic in this study, there was no uniform trend in the associations. Moreover, ions, metallic elements, and PAHs were differentially associated with genotoxic damage produced by cellular exposure to different doses of PM. Previous studies found that most of the PAHs in PM samples were highly genotoxic (Bai et al., 2017; Dat and Chang, 2017). However, the results of this study suggest that PAHs were not the only factor affecting genotoxicity, and that the PM dose had a large effect on genotoxicity. Furthermore, not all chemical constituents contribute to the overall toxicity (including genotoxicity) of PM in this study. The mixture of toxic constituents and their individual contributions to the toxicological profile of PM remain largely unknown (Jin et al., 2017).

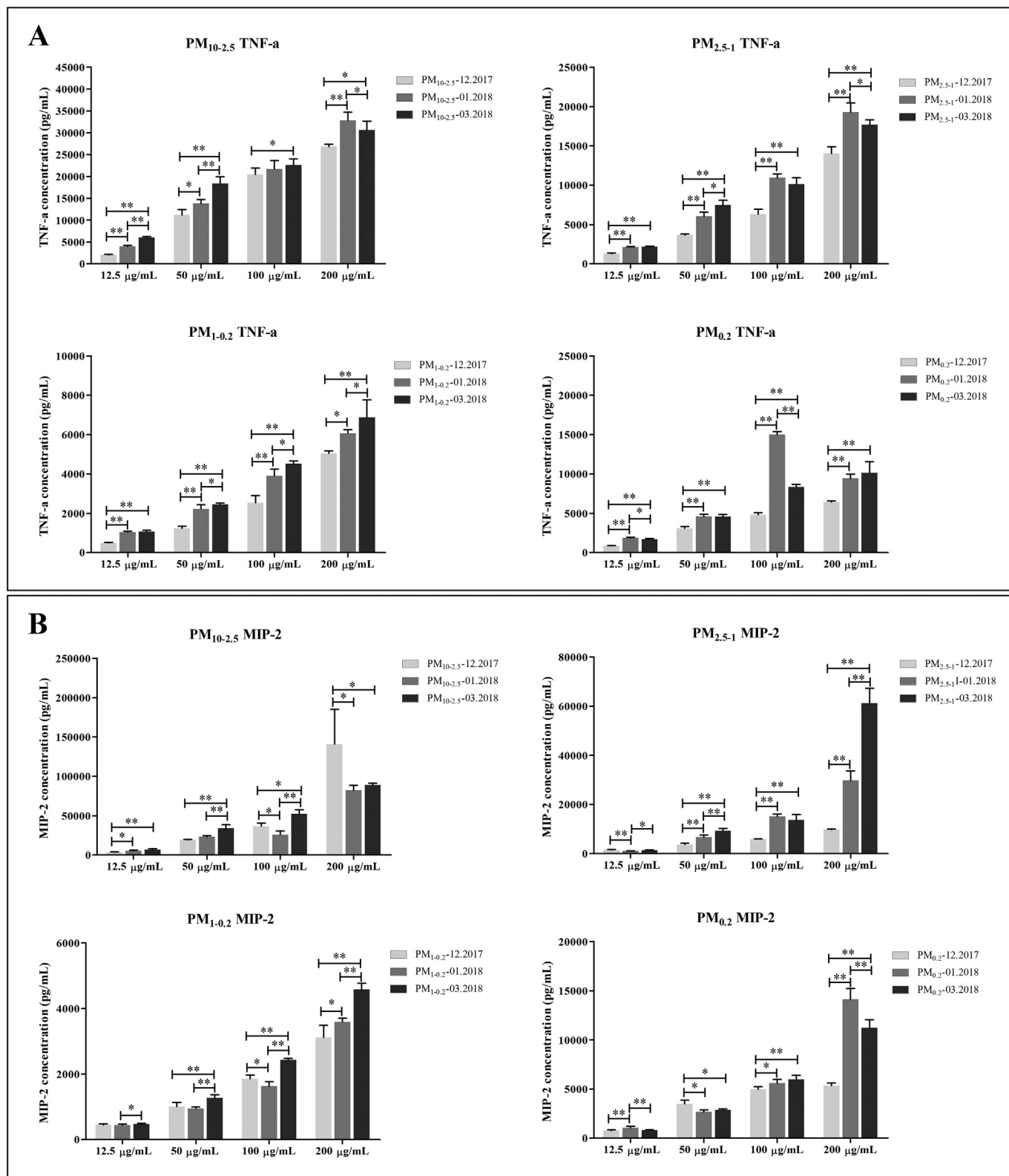


Fig. 9. Tumor necrosis factor alpha (TNF-a) and Macrophage inflammatory protein 2 (MIP-2) production in RAW 264.7 macrophages after exposure to four doses of size-segregated particulate samples in December 2017, January 2018 and March 2018. * $P < 0.05$, ** $P < 0.001$.

Inflammation is considered to be a key mechanism of PM-induced disease (Zhang et al., 2020). TNF- α is a classical pleiotropic pro-inflammatory cytokine (Sethi and Hotamisligil, 2021). One of the hallmarks of acute inflammatory states is the recruitment and activation of polymorphonuclear leukocytes, in which TNF- α has been shown to be

involved (Klebanoff et al., 1986). In this study, all four particle sizes caused dose-dependent increases in TNF- α in winter and spring, with PM_{10-2.5} exposure causing the highest TNF- α expression. This is consistent with the results of Rönkkö et al. (Rönkkö et al., 2018) and Pasi et al. (Jalava et al., 2015b). The ions and PAHs content of PM_{10-2.5} was less than for

Table 2
Associations of PM components with toxicological endpoints in RAW 264.7 macrophages.

Items	12.5 µg/mL			50 µg/mL			100 µg/mL			200 µg/mL		
	Ions	TE	PAHs	Ions	TE	PAHs	Ions	TE	PAHs	Ions	TE	PAHs
PM _{10-2.5}												
MTT			0.64*	0.68*					0.79**			0.55*
Sub G1/G0			0.79*	0.90**			0.95**			0.84*		
DNA Tail-I				-0.66*	0.76**		-0.59*	0.67*		0.84**	-0.58*	
DCF	-0.95**			-0.84*					-0.67*			-0.71*
TNF-α	0.95**			0.94**			0.54*			0.57*		0.84**
MIP-2	0.86**			0.95**				-0.95**				-0.87**
PM _{2.5-1}												
MTT		0.79**		0.56*				0.74*			0.79**	
Sub G1/G0	0.69*			0.79*				0.95**			0.95**	
DNA Tail-I		-0.88**	-0.54*	-0.50*	-0.92**		-0.58*	-0.84**		-0.70**		0.60*
DCF		-0.85*				-0.74*	0.74*	0.05	-0.69*			-0.90**
TNF-α	0.86**	0.71*		0.94**			0.56*	0.85**		0.51*	0.94**	0.51*
MIP-2		-0.81**	-0.69*	0.94**			0.62*	0.80*		0.94**		
PM _{1-0.2}												
MTT								0.73*				-0.77**
Sub G1/G0	0.72*					-0.84*		0.95**				-0.95**
DNA Tail-I		-0.85**	0.56*	-0.84**		0.58*	-0.94**	0.47*				
DCF						-0.69*		0.74*				-0.69*
TNF-α		0.63*	-0.79**		0.58*	-0.84**						-0.83**
MIP-2	0.60*			0.70*		-0.71*	0.89**		-0.53*			-0.85**
PM _{0.2}												
MTT												
Sub G1/G0	0.69*	0.69*	-0.69*	-0.95**	-0.95**	0.95**				-0.53*	-0.53*	0.53*
DNA Tail-I				0.47*	0.47*	-0.47*						
DCF	0.84*	0.84*	-0.84*	0.95**	0.95**	-0.95**	0.79*	0.79*	-0.79*	0.79*	0.79*	-0.79*
TNF-α							-0.60*	-0.60*	0.60*			
MIP-2	-0.60*	-0.60*	0.60*									

The values are Spearman's correlation coefficients (ρ). Asterisks indicate statistical significance * ($P < 0.05$) and ** ($P < 0.001$). TE: total elements; PAHs: polycyclic aromatic hydrocarbons; DNA Tail-I: DNA Tail-Intensity.

other particles, although metals content was greater. Interestingly, ions and PAHs in PM_{10-2.5} were significantly positively associated with TNF- α expression, whereas metals were not significantly associated with TNF- α . It is difficult to interpret these results from the content of PM_{10-2.5} components and their associations with TNF- α , but high oxidative damage caused by PM_{10-2.5} exposure may be a key factor in the high expression of TNF- α . MIP-2 is secreted by endotoxin-stimulated macrophages, has an affinity for heparin-binding protein, and is an inflammatory protein that induces local inflammatory responses (Wolpe et al., 1989). MIP-2 is chemotactic to human polymorphonuclear leukocytes, but does not induce chemotaxis or an oxidative burst (Wolpe et al., 1989). MIP-2 generally represented 0.5 % of the protein secreted by endotoxin-stimulated RAW 264.7 cells (Wolpe et al., 1989). All PM samples caused dose-dependent increases in MIP-2 in this study, and the expression of MIP-2 was about 5 times greater than that of TNF- α . Previous studies have also found higher expression of MIP-2 than that of TNF- α and IL-6 in RAW 264.7 cells exposed to PM (Jalava et al., 2006). We did not measure endotoxin levels in the PM samples in this study, but we found that other chemical constituents (such as ions and PAHs) of PM were significantly associated with MIP-2 production.

SO₄²⁻, NO₃⁻ and NH₄⁺ are primary chemical components of PM, and accounted for a large proportion of PM components in this study, especially in the small-sized PM_{0.2}. Particles from different source classes have been shown to produce different biological effects *in vitro* (Grilli et al., 2018).

In this study, the main source of PM_{10-2.5} was soil dust, especially in winter. Dry seasons in winter and early spring were responsible for soil dust being the main source of PM. Biomass burning is the main source of PM_{2.5-1} and PM_{1-0.2}, especially in spring. Biomass burning begins in late winter and spring in rural areas, leading to the increased contribution of biomass burning to PM. The Sun Yat-sen University campus is adjacent to Dongfeng East Road in the north and Zhixin South Road in the east, with heavy traffic and a lot of residential buildings and restaurants. Therefore, the dust carried by the car, cooking and fuel combustion may be the reasons that cause soil dust and biomass burning to be the main source of PM. Moreover, Guangdong Province has 4.41×10^4 km² of cultivated field and 9.3×10^4 km² of forest area (based on 2006 statistics), which produces

a large number of agricultural residues and firewood that is used as biofuel, especially in rural areas and dry season (Zhang et al., 2010). And, over half of the rural households in Guangdong Province, >90 % use biofuels for cooking and/or heating (Zhang et al., 2010). Therefore, biomass burning accounted for a larger proportion of PM sources from December 2017 to March 2018. The main sources of PM_{0.2} in this study were traffic exhaust and coal combustion. The impact of transboundary air pollution on urban-level PM-related public health effects in the PRD is affected by the seasons. For example, the large-scale fogs and hazes in central and eastern of China in mid-January 2013 caused serious air pollution in North China, Central China, and the PRD region (Fan et al., 2015). Previous studies reported that transboundary air pollution between different cities is a main cause of air pollution in the PRD region (Gu and Yim, 2016; Luo et al., 2018; Tong et al., 2018). A 2013 study reported that about 8.6 % of the PM_{2.5} level in Guangzhou could be attributed to mobile sources from adjacent regions (Dongguan, Foshan, and Shenzhen) (Wu et al., 2013). Heating in northern Chinese cities usually lasts until May. Therefore, the high seasonal mean PM observed in Guangzhou's winter and spring may be due in part to high winter heating emissions and/or poor dispersion and elimination of pollutants from other areas, even in the unheated PRD region of southern China. We also found that the contributions of the five sources to four size particles was different. This is attributed to the local geographic climate and the complex formation process of particles of different sizes (Rönkkö et al., 2018).

In addition to the primary emissions, secondary aerosols may be formed in the atmosphere, either as new ultrafine particles or as condensates on the existing particles (Tao et al., 2017). In the PRD region, secondary inorganic aerosols (SO₄²⁻, NO₃⁻ and NH₄⁺) accounted for 33–38 % of the 2002–2003 annual PM_{2.5}. In rural areas outside of Guangzhou, secondary inorganic aerosols accounted for 35–48 % of the 2002–2003 PM_{2.5} mass. The annual SO₄²⁻, NO₃⁻ and NH₄⁺ concentrations of PM_{2.5} in Guangzhou were decreased from 2010 to 2014 due to the implementation of power plant flue gas desulfurization facilities and large industrial boilers in Guangdong Province (Tao et al., 2017), but the SO₄²⁻, NO₃⁻ and NH₄⁺ concentrations in the suburban areas of Guangzhou were increased (Lai et al., 2016). The

contribution of biomass burning to $PM_{0.2}$ was large in winter and spring in this study. Therefore, biomass burning in rural/suburban areas may play an important role in governing the concentrations of SO_4^{2-} , NO_3^- and NH_4^+ in particles. We also found that the total amount of ions in Guangzhou in spring was relatively high. This is because the seasonal contributions of secondary inorganic aerosols in spring and autumn in Guangzhou were generally higher than that in summer and winter (Tao et al., 2017).

In this study, the total particle content of metallic elements was higher in winter than in spring. Previous studies also found greater metallic element concentrations in Guangzhou PM during winter than spring (Li et al., 2016). This may result from soil dust and coal combustion contributions during winter but not in spring. There is a relatively stable contribution from industrial sources, but we found that the contribution percentage of industrial sources has half as great in spring PM than in winter PM. China has carried out a large number of emission reduction projects related to $PM_{2.5}$ and other related air pollutants in the past ten years (Yu et al., 2019), and these emission reduction projects have strict, local-specific requirements on industrial emissions. Unfortunately, most studies focused on evaluating the average annual decline in $PM_{2.5}$ (including components) and other air pollutants (Feng et al., 2019; Yu et al., 2019), and did not compare evaluate the contribution of industrial emissions to PM after the implementation of emission reduction policies and in different seasons. Industrial exhaust is usually emitted at a high altitude, an is susceptible to wind and other climate factors (Miettinen et al., 2019). Guangzhou usually begins to enter the summer (rainy season) after March, and the change of seasons may have contributed to the diminished impact of industrial sources on spring PM. More research and evidence are needed to investigate the contribution of industrial sources to PM in different seasons.

The metallic elements investigated in this study come mainly from industrial and traffic emissions (Reff et al., 2009). Si was the most abundant metal in this study, and is generally considered to be a toxic marker of mineral dust components that is also related to traffic emissions (Reff et al., 2009). Soil dust usually increases during the warm and dry seasons; winter is the dry season in Guangzhou (Lai et al., 2016). In this study, traffic exhaust made a large contribution to spring PM, but industrial and soil dust sources played greater role in the content of metallic elements in winter PM samples.

Organic matter is also a major component of PM in PRD (Tao et al., 2017). The total PAH concentrations in winter and spring were 1460.68 ng/mg and 1009.23 ng/mg, respectively. This seasonal difference is consistent with the typical study findings from urban atmospheres, which were affected by increase at sources of pollution during winter (Guo et al., 2003). Meteorological conditions, such as lower boundary layer heights and lower horizontal wind speeds, are often the factors controlling pollutant accumulation in winter (Wang et al., 2016). In this study, FA was the most abundant PAH in $PM_{10-2.5}$ and $PM_{2.5-1}$, with mass concentrations of 33.05 and 38.11 ng/mg in $PM_{10-2.5}$, respectively, and 45.76 and 45.04 ng/mg in $PM_{2.5-1}$ on average, respectively; accounting for 26.8 % and 30.4 % in $PM_{10-2.5}$, and 17.4 % and 24.0 % in $PM_{2.5-1}$ of total PAHs in winter and spring, respectively. B(b)FA was the most abundant PAH in winter and spring $PM_{1-0.2}$ (average mass concentrations of winter: 50.89 ng/mg, and spring: 34.99 ng/mg), and winter $PM_{0.2}$ (average mass concentrations of 85.02 ng/mg). FA and B(b)FA are often used as markers for carcinogenic risk assessment. The PAHs levels in this study were lower than those previously reported by the South China Institute of Environmental Sciences for an urban area of Guangzhou during winter and summer 2012/2013 (Wang et al., 2016). However, PAH concentrations in most of the PM samples in this study exceeded the 1.0 ng/m^3 air quality guidelines set by the World Health Organization (WHO) (Wang et al., 2016), especially for $PM_{1-0.2}$, indicating a potential health risk in the region, and suggesting that the detection of small particle size fraction chemical components should be strengthened.

The strengths of this study were collection of four particle size fractions ($PM_{10-2.5}$, $PM_{2.5-1}$, $PM_{1-0.2}$, $PM_{0.2}$) in Guangzhou during winter 2017 and spring 2018, and thoroughly measuring their chemical components. We analyzed and compared the differences between the toxicity of four particle

size fractions collected during two seasons, adding evidence to help understand the potential health hazardous aspects of exposure to the particles and their effects on the public health. The limitation of this study was that we did not analyze the source of the components of different size fraction particles in each season due to an insufficient number of samples. In order to fully leverage the collection efficiency of each filter, we collected samples during 24–72 h interval with only 10–15 of samples collected each month. Thus, our sample number was insufficient for a particle source analysis, although we can collect four size fraction particles in each sampling. In addition, due to the differences in calculation and calibration methods, the ion concentration we detected and calculated are generally higher than previously reported levels.

5. Conclusion

In conclusion, Guangzhou PM mass concentrations were higher during winter and caused more severe cytotoxicity and oxidative damage compared to the PM collected during spring when the same mass dose was compared. Exposure to PM collected in winter and spring led to an increased proportion of RAW264.7 cells in arrested in the Sub-G1/G0 phase and genotoxicity. The trends in the components of size-segregated PM samples from winter and spring were consistent. PM Metallic elements and PAHs were greatest in winter and PM ions were greatest in spring. Metallic elements, PAHs and ions in the size-segregated PM samples were associated with almost all toxicological endpoints. Soil dust and biomass burning were the main sources contributing to PM in winter, whereas traffic exhaust and biomass burning was the main source contributing to PM in spring. Our results suggest that during winter and spring, the composition of the PM samples in Guangzhou across different size ranges led to strong variations in toxicological responses. The present study demonstrated the importance of examining a variety of particle sizes, compositions and sources across different seasons.

Supplementary data to this article can be found online at <https://doi.org/10.1016/j.scitotenv.2022.157382>.

CRediT authorship contribution statement

Mo Yang: Conceptualization, Methodology, Validation, Formal analysis, Investigation, Writing – original draft, Writing – review & editing, Resources, Data curation, Supervision. **Pasi Jalava:** Conceptualization, Methodology, Validation, Writing – original draft, Writing – review & editing, Funding acquisition, Resources. **Xin-Feng Wang:** Methodology, Formal analysis, Investigation, Writing – review & editing. **Michael S. Bloom:** Writing – review & editing. **Ari Leskinen:** Methodology, Writing – review & editing. **Henri Hakkarainen:** Methodology, Writing – review & editing. **Marjut Roponen:** Methodology. **Mika Komppula:** Methodology. **Qi-Zhen Wu:** Methodology, Data curation. **Shu-Li Xu:** Methodology, Data curation. **Li-Zi Lin:** Formal analysis, Investigation. **Ru-Qing Liu:** Formal analysis, Investigation, Funding acquisition. **Li-Wen Hu:** Formal analysis, Investigation, Funding acquisition. **Bo-Yi Yang:** Formal analysis, Investigation, Funding acquisition. **Xiao-Wen Zeng:** Conceptualization, Methodology, Funding acquisition. **Yun-Jiang Yu:** Conceptualization, Methodology, Writing – review & editing. **Guang-Hui Dong:** Conceptualization, Methodology, Validation, Writing – original draft, Writing – review & editing, Funding acquisition, Resources, Supervision.

Declaration of competing interest

The authors declare that they have no known competing financial interests or personal relationships that could have appeared to influence the work reported in this paper.

Acknowledgements

This work was supported by the National Key Research and Development Program of China (grant number 2018YFE0106900),

National Natural Science Foundation of China (grant numbers M-0420, 82130094, 82103823, 82073502, 81872582, 81872583, 81972992), the Science and Technology Program of Guangzhou (grant numbers 201807010032, 201803010054), Guangdong Provincial Natural Science Foundation Team Project (grant number 2018B030312005), Fundamental Research Funds for the Central Universities (grant number 19ykjc01), Natural Science Foundation of Guangdong Province (grant numbers 2021B1515020015, 2021A1515011754, 2021A1515012212, 2020A1515011131, 2019A050510017, 2018B05052007, 2017A090905042), Medical Scientific Research Foundation of Guangdong Province (grant number 20201123193141971), Academy of Finland (grant numbers 287982, 294081, 319245).

References

- Alas, H.D.C., et al., 2019. Methodology for high-quality mobile measurement with focus on black carbon and particle mass concentrations. *Atmos. Meas. Tech.* 12, 4697–4712.
- Arruti, A., et al., 2011. Impact of the global economic crisis on metal levels in particulate matter (PM) at an urban area in the Cantabria region (Northern Spain). *Environ. Pollut.* 159, 1129–1135.
- Bai, H., et al., 2017. Chronic polycyclic aromatic hydrocarbon exposure causes DNA damage and genomic instability in lung epithelial cells. *Oncotarget* 8, 79034.
- Dat, N.-D., Chang, M.B., 2017. Review on characteristics of PAHs in atmosphere, anthropogenic sources and control technologies. *Sci. Total Environ.* 609, 682–693.
- Fan, Q., et al., 2015. Process analysis of regional aerosol pollution during spring in the Pearl River Delta region, China. *Atmos. Environ.* 122, 829–838.
- Fang, D., et al., 2019. Chemical composition and health risk indices associated with size-resolved particulate matter in Pearl River Delta (PRD) region, China. *Environ. Sci. Pollut. Res.* 26, 12435–12445.
- Feng, D., 2021a. Short-term effects of particle sizes and constituents on blood biomarkers among healthy young adults in Guangzhou, China. *Environ. Sci. Technol.* 55, 5636–5647.
- Feng, Y., et al., 2019. Defending blue sky in China: effectiveness of the “Air pollution prevention and control action plan” on air quality improvements from 2013 to 2017. *J. Environ. Manag.* 252, 109603.
- Feng, D., et al., 2021b. Associations between size-fractionated particulate matter and left ventricular voltage: a panel study among healthy young adults in southern China. *Atmos. Environ.* 254, 118395.
- Feng, R., et al., 2022. Quantifying influences of administrative division adjustment on PM_{2.5} pollution in China's mega-urban agglomerations. *J. Environ. Manag.* 302, 113993.
- Genies, C., et al., 2016. Inhibition of the formation of benzo [a] pyrene adducts to DNA in A549 lung cells exposed to mixtures of polycyclic aromatic hydrocarbons. *Toxicol. in Vitro* 35, 1–10.
- Ghio, A.J., et al., 2012. Composition of air pollution particles and oxidative stress in cells, tissues, and living systems. *J. Toxicol. Environ. Health Part B* 15, 1–21.
- Griffith, S.M., et al., 2015. Characterizing the thermodynamic and chemical composition factors controlling PM_{2.5} nitrate: insights gained from two years of online measurements in Hong Kong. *Atmos. Environ.* 122, 864–875.
- Grilli, A., et al., 2018. Transcriptional profiling of human bronchial epithelial cell BEAS-2B exposed to diesel and biomass ultrafine particles. *BMC Genomics* 19, 1–15.
- Gu, Y., Yim, S.H.L., 2016. The air quality and health impacts of domestic trans-boundary pollution in various regions of China. *Environ. Int.* 97, 117–124.
- Guo, H., et al., 2003. Particle-associated polycyclic aromatic hydrocarbons in urban air of Hong Kong. *Atmos. Environ.* 37, 5307–5317.
- Guo, P.Y., et al., 2021. Short-term effects of particle size and constituents on blood pressure in healthy young adults in Guangzhou, China. *J. Am. Heart Assoc.* 10, e019063.
- He, Z.-Z., et al., 2021. Associations of particulate matter sizes and chemical constituents with blood lipids: a panel study in Guangzhou, China. *Environ. Sci. Technol.* 55, 5065–5075.
- Hu, W., et al., 2021. Ambient particulate matter compositions and increased oxidative stress: exposure-response analysis among high-level exposed population. *Environ. Int.* 147, 106341.
- Huang, D., et al., 2012. Valuing the health risks of particulate air pollution in the Pearl River Delta, China. *Environ. Sci. Pol.* 15, 38–47.
- Jalava, P.I., et al., 2006. In vitro inflammatory and cytotoxic effects of size-segregated particulate samples collected during long-range transport of wildfire smoke to Helsinki. *Toxicol. Appl. Pharmacol.* 215, 341–353.
- Jalava, P., et al., 2015a. Day and night variation in chemical composition and toxicological responses of size segregated urban air PM samples in a high air pollution situation. *Atmos. Environ.* 120, 427–437.
- Jalava, P.I., et al., 2015b. Chemical and microbial components of urban air PM cause seasonal variation of toxicological activity. *Environ. Toxicol. Pharmacol.* 40, 375–387.
- Jin, L., et al., 2017. Airborne particulate matter pollution in urban China: a chemical mixture perspective from sources to impacts. *Natl. Sci. Rev.* 4, 593–610.
- Jin, L., et al., 2019. Contributions of city-specific fine particulate matter (PM_{2.5}) to differential in vitro oxidative stress and toxicity implications between Beijing and Guangzhou of China. *Environ. Sci. Technol.* 53, 2881–2891.
- Kalisa, E., et al., 2019. Chemical and biological components of urban aerosols in Africa: current status and knowledge gaps. *Int. J. Environ. Res. Public Health* 16, 941.
- Kelly, F.J., 2003. Oxidative stress: its role in air pollution and adverse health effects. *Occup. Environ. Med.* 60, 612–616.
- Kim, M.-S., et al., 2021. Assessment of pollution sources and contribution in urban dust using metal concentrations and multi-isotope ratios (13C, 207/206Pb) in a complex industrial port area, Korea. *Atmosphere* 12, 840.
- Klebanoff, S., et al., 1986. Stimulation of neutrophils by tumor necrosis factor. *J. Immunol.* 136, 4220–4225.
- Kroll, A., et al., 2013. In vitro toxicology of ambient particulate matter: correlation of cellular effects with particle size and components. *Environ. Toxicol.* 28, 76–86.
- Lai, S., et al., 2016. Characterization of PM_{2.5} and the major chemical components during a 1-year campaign in rural Guangzhou, Southern China. *Atmos. Res.* 167, 208–215.
- Li, Y., et al., 2016. Characteristics, sources and health risk assessment of toxic heavy metals in PM_{2.5} at a megacity of Southwest China. *Environ. Geochem. Health* 38, 353–362.
- Li, M., et al., 2020. Nitrated phenols and the phenolic precursors in the atmosphere in urban Jinan, China. *Sci. Total Environ.* 714, 136760.
- Longhin, E., et al., 2013. Season linked responses to fine and quasi-ultrafine Milan PM in cultured cells. *Toxicol. in Vitro* 27, 551–559.
- Longhin, E.M., et al., 2020. Fifteen years of airborne particulates in vitro toxicology in Milano: lessons and perspectives learned. *Int. J. Mol. Sci.* 21, 2489.
- Lu, X., et al., 2017. Assessment of health burden caused by particulate matter in southern China using high-resolution satellite observation. *Environ. Int.* 98, 160–170.
- Luo, M., et al., 2018. Trans-boundary air pollution in a city under various atmospheric conditions. *Sci. Total Environ.* 618, 132–141.
- Manzano-León, N., et al., 2016. TNF α and IL-6 responses to particulate matter in vitro: variation according to PM size, season, and polycyclic aromatic hydrocarbon and soil content. *Environ. Health Perspect.* 124, 406–412.
- Miettinen, M., et al., 2019. PM_{2.5} concentration and composition in the urban air of Nanjing, China: effects of emission control measures applied during the 2014 youth olympic games. *Sci. Total Environ.* 652, 1–18.
- Motoyama, Y., et al., 2009. Oxidative stress more strongly induced by ortho-than Para-quinoid polycyclic aromatic hydrocarbons in A549 cells. *J. Health Sci.* 55, 845–850.
- Park, M., et al., 2018. Differential toxicities of fine particulate matters from various sources. *Sci. Rep.* 8, 1–11.
- Park, S., et al., 2022. Potential toxicity of inorganic ions in particulate matter: ion permeation in lung and disruption of cell metabolism. *Sci. Total Environ.* 824, 153818.
- Polissar, A.V., et al., 1998. Atmospheric aerosol over Alaska: 2. Elemental composition and sources. *J. Geophys. Res. Atmos.* 103, 19045–19057.
- Reff, A., et al., 2009. Emissions inventory of PM_{2.5} trace elements across the United States. *Environ. Sci. Technol.* 43, 5790–5796.
- Rönkkö, T.J., et al., 2018. Emissions and atmospheric processes influence the chemical composition and toxicological properties of urban air particulate matter in Nanjing, China. *Sci. Total Environ.* 639, 1290–1310.
- Rönkkö, T.J., et al., 2021. Inflammatory responses of urban air PM modulated by chemical composition and different air quality situations in Nanjing, China. *Environ. Res.* 192, 110382.
- Samet, J.M., et al., 2020. Non-redox cycling mechanisms of oxidative stress induced by PM metals. *Free Radic. Biol. Med.* 151, 26–37.
- Sethi, J.K., Hotamisligil, G.S., 2021. Metabolic messengers: tumour necrosis factor. *Nat. Metab.* 3, 1302–1312.
- Song, Y., et al., 2020. The cellular effects of PM_{2.5} collected in Chinese Taiyuan and Guangzhou and their associations with polycyclic aromatic hydrocarbons (PAHs), nitro-PAHs and hydroxy-PAHs. *Ecotoxicol. Environ. Saf.* 191, 110225.
- Tao, J., et al., 2017. Source apportionment of PM_{2.5} at urban and suburban areas of the Pearl River Delta region, South China-with emphasis on ship emissions. *Sci. Total Environ.* 574, 1559–1570.
- Tong, C.H.M., et al., 2018. Assessing the impacts of seasonal and vertical atmospheric conditions on air quality over the Pearl River Delta region. *Atmos. Environ.* 180, 69–78.
- Velali, E., et al., 2018. In vitro cellular toxicity induced by extractable organic fractions of particles exhausted from urban combustion sources-role of PAHs. *Environ. Pollut.* 243, 1166–1176.
- Wang, J., et al., 2016. Characterization of PM_{2.5} in Guangzhou, China: uses of organic markers for supporting source apportionment. *Sci. Total Environ.* 550, 961–971.
- Wang, M., et al., 2019. Source contributions of surface ozone in China using an adjunct sensitivity analysis. *Sci. Total Environ.* 662, 385–392.
- Wolpe, S.D., et al., 1989. Identification and characterization of macrophage inflammatory protein 2. *Proc. Natl. Acad. Sci.* 86, 612–616.
- Wu, D., et al., 2013. A study of control policy in the Pearl River Delta region by using the particulate matter source apportionment method. *Atmos. Environ.* 76, 147–161.
- Yang, L., et al., 2016. Pro-inflammatory response and oxidative stress induced by specific components in ambient particulate matter in human bronchial epithelial cells. *Environ. Toxicol.* 31, 923–936.
- Yu, M., et al., 2019. Effects of air pollution control measures on air quality improvement in Guangzhou, China. *J. Environ. Manag.* 244, 127–137.
- Zhang, Z., et al., 2010. Chemical speciation, transport and contribution of biomass burning smoke to ambient aerosol in Guangzhou, a mega city of China. *Atmos. Environ.* 44, 3187–3195.
- Zhang, J., et al., 2018. Trace elements in PM_{2.5} in Shandong Province: source identification and health risk assessment. *Sci. Total Environ.* 621, 558–577.
- Zhang, Q., et al., 2020. The acute effects of fine particulate matter constituents on circulating inflammatory biomarkers in healthy adults. *Sci. Total Environ.* 707, 135989.
- Zhou, M., et al., 2019. Mortality, morbidity, and risk factors in China and its provinces, 1990–2017: a systematic analysis for the global burden of disease study 2017. *Lancet* 394, 1145–1158.